Incident-Angle-Dependent Reflectance in Distributed Bragg Reflectors Fabricated from ZnO/MgO Multilayer Films

Ying-Shin HUANG, Sheng-Yao HU, Chia-Chih HUANG, Yueh-Chien LEE, Jyh-Wei LEE, Chung-Cheng CHANG, Zin-Kuan WUN, and Kwong-Kau TIONG

OPTICAL REVIEW Vol. 21, No. 5 (2014)

OPTICAL REVIEW Vol. 21, No. 5 (2014) 651–654

Incident-Angle-Dependent Reflectance in Distributed Bragg Reflectors Fabricated from ZnO/MgO Multilayer Films

Ying-Shin Huang[1], Sheng-Yao Hu[2], Chia-Chih Huang[3], Yueh-Chien Lee[3*], Jyh-Wei Lee[4], Chung-Cheng Chang[1], Zin-Kuan Wun[1], and Kwong-Kau Tiong[1]

[1]*Department of Electrical Engineering, National Taiwan Ocean University, Keelung 20224, Taiwan*
[2]*Department of Digital Technology Design, Tungfang Design University, Hunei, Kaohsiung 82941, Taiwan*
[3]*Department of Electronic Engineering, Tungnan University, Shenkeng, New Taipei City 22202, Taiwan*
[4]*Department of Materials Engineering, Ming Chi University of Technology, Taishan, New Taipei City 24301, Taiwan*

(Received March 30, 2014; Accepted June 27, 2014)

We present the incident-angle-dependent reflectance spectra of the 10-period ZnO/MgO multilayer films deposited on Si by sputtering technique. As increasing the incident angle, the resonant wavelength and bandwidth of the measured reflectance spectra exhibit redshift and narrower, respectively. The theoretical curves using transfer matrix method taken account of transverse electric (TE) and transverse magnetic (TM) polarizations are calculated to well describe the variations in the behavior of the experimental spectra. The simulated TE- and TM-reflection band at different angles can evaluate the bandwidth of the resonance band and provide valuable parameters to design an omnidirectional-reflection band in selected multilayer structure.

Keywords: zinc oxide, distributed Bragg reflectors, reflectance, sputtering

1. Introduction

Zinc oxide (ZnO) semiconductor material with a wide band gap of 3.37 eV and an exciton binding energy of 60 meV at room temperature has attracted much attention for electronics and optoelectronics devices such as sensors, solar cells, detectors, and light emitting diodes (LEDs).[1,2] Recently, ZnO-based distributed Bragg reflectors (DBRs) are further applied in increasing the efficiency of LEDs or vertical cavity surface emitting laser (VCSEL) with an emission range below the band gap of ZnO material.[3,4]

The DBRs constructed from a periodic multi-layered stack by using two different materials with different refractive indices are widely used in optoelectronic devices.[5] The thickness of the high- and the low-refractive index (n) layers are determined by the designed resonant wavelength of reflection band according to the formula of $\lambda/4n$. It is also known that the reflectance band of DBRs depends on the difference between the refractive indices (Δn) of two alternating materials and the number of repeated pairs (N) of low/high refractive index material.[6]

To clarify the incident-angle-dependent reflectance spectrum of DBRs and further extend its applications to be a multilayer omnidirectional reflector, then an overlapping reflectance band to all spectra can be taken at any incident angles.[7] In addition, the bandwidth of the omnidirectional reflectance band would be limited by the reflectance band for the transverse electric (TE) and transverse magnetic (TM) waves propagating in the multilayer structure. Therefore, a detailed analysis for TE and TM polarizations propagating in the DBRs as a function of incident angle is necessary to design an absolute omnidirectional band.

In this work, both of wide-band-gap materials of zinc oxide (ZnO) and magnesium oxide (MgO) materials are selected to construct a multilayer structure with the maximum Δn of about 0.4 which might be considered for the DBRs structure in the application of ultraviolet (UV) optoelectronic devices. We fabricate the 10-period ZnO/MgO multilayer films on Si substrate by sputtering technology and measure the incident-angle-dependent reflectance spectra of the prepared samples. The experimental reflectance spectra are further compared with the theoretical ones by using the transfer matrix method. The variations in the resonant wavelength and bandwidth of reflectance band are also investigated by the simulated curves in terms of incident angle for TE and TM polarizations.

2. Experimental Procedure

To avoid the absorption effect in the performance of DBRs, the resonant wavelength of ZnO/MgO multilayer films is designed to be at 550 nm. It has been known that ZnO with a wurtzite crystal structure is optically uniaxial, defined by a dielectric function for light polarized parallel to the c-axis (extraordinary, n_e) and by a dielectric function for light polarized perpendicular to the c-axis (ordinary, n_o). Thus, the material has anisotropic optical properties.[2,8] By taking the ordinary index into account with the Sellmeir equation, the reflective indices for the designed resonant wavelength can be obtained as 2.013 for ZnO and 1.710 for MgO.[9,10] Furthermore, the estimated thickness in each individual layer for ZnO was 68.3 nm and for MgO was 80.5 nm.

The 10-period ZnO/MgO multilayer films were grown on the p-type (100) silicon wafer by reactive magnetron sputtering system. The direct current (DC) and radio frequency (RF) power supplies were connected to a ZnO compound target and a pure Mg target, respectively. The diameter and thickness of each target were 76.2 and 6.0 mm, respectively. The substrate-to-target distance was kept at 85 mm. The base pressure, 6.65×10^{-4} Pa was achieved

*E-mail address: jacklee@mail.tnu.edu.tw

Table 1. Detailed deposition parameters for ZnO/MgO multilayer thin films.

	ZnO	MgO
Substrate	Si	
Target	ZnO	Mg
Sputtering method	DC	RF
Gas flow (sccm)	Ar:25, O_2:25	
Working pressure (Pa)	1.73×10^{-1}	
Sputtering power (W)	50	150
Substrate temperature (°C)	300	

before sputtering and the working pressure during sputtering was 1.73×10^{-1} Pa. the flow rate of $Ar : O_2$ at a ratio of 1 : 1 was monitored by individual mass flow controllers. All substrates were heated to 300 °C and rotated at a speed of 20 rpm during the sputtering process. Before the multilayer films deposition, monolayers of ZnO and MgO were fabricated, respectively, to determine the corresponding deposition rate. Therefore, the thickness control of ZnO and MgO layers can be achieved through a proper control of shutters on/off time for ZnO and Mg targets. For the 10-period ZnO/MgO multilayer films deposition, the 300 nm thick ZnO buffer layer was deposited on the Si substrate first, and then the desired thickness MgO layer and ZnO layer were sequentially deposited to fabricate the 10-period ZnO/MgO multilayer films. Detailed deposition parameters are listed in Table 1.[11)]

The structural properties of the prepared ZnO/MgO multilayer films were characterized by a glancing angle X-ray diffractometer (GA-XRD; PANalytical X'pert) with an incidence angle of 1° and the Cu Kα radiation generated at 30 kV and 20 mA from a Cu target was used. The cross-section morphology was obtained by a field emission scanning electron microscope (FE-SEM; JEOL JSM-6701F). The reflectance spectrum of ZnO/MgO multilayer films was measured at different incidence angles of 0, 30, 45, and 60°. The Xenon lamp was used as the light source and the reflected beam was dispersed through a 0.5 m spectrometer (Zolix omni-λ 500) with a grating of 1200 grooves/mm and detected by using a photomultiplier tube.

3. Results and Discussion

Figure 1(a) shows the XRD spectrum of the 10-period ZnO/MgO multilayer films and presents the designed diffraction peaks for ZnO and MgO materials referred to JCPDS No. 89-7102 and JCPDS No. 89-7746.[12,13)] A typical diffraction peak of (002) for the hexagonal phase of ZnO and that of (200) for the cubic phase of MgO can significantly be observed. It also catches the attention that the XRD signals at about 36 and 62°, respectively, can be attributed to the (101) and (103) for ZnO or the (111) and (220) for MgO.[12,13)] As a result, the 10-period ZnO/MgO multilayer films were fabricated successfully.

The cross-sectional SEM morphology of the 10-period ZnO/MgO multilayer films is shown in Fig. 1(b). It can be observed that the laminated structure illustrates the multi-

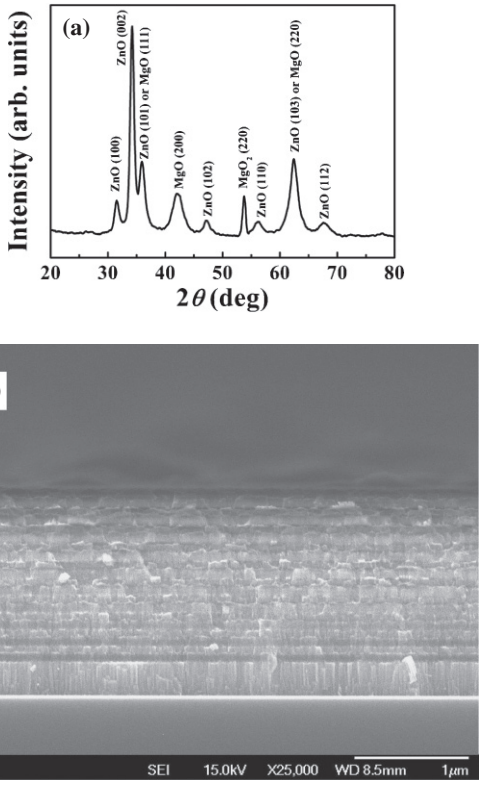

Fig. 1. (a) XRD patterns and (b) cross-sectional SEM image of 10-period ZnO/MgO multilayer films.

layer microstructure consisting of bright ZnO and gray MgO layers. From the SEM images, the estimated average thickness is about 69.6 nm for ZnO layers and 72.3 nm for MgO layers, where are derived from the designed thickness. Additionally, the SEM image also shows the manifestation of waviness at the interface between the ZnO and MgO layer, which has been known as the large lattice mismatch between ZnO and MgO materials.[6)] The undesired thickness and unstable interface mean that there is a challenge to control the growth rate of a nanolayer by using the sputtering technology.

The reflectance spectra of the 10-period ZnO/MgO multilayer films at the incident angle of 0, 30, 45, and 60° are measured and shown in Fig. 2(a). For the incident angle of 0°, the reflectance spectrum shows an asymmetric shape and the stop-band center is about at 561 nm, which is longer than the designed resonant wavelength of 550 nm. The origin of the shift has been investigated by taking account of wavelength-dependent refractive index and the distributed random thickness in previous report.[11)] In this work, two obvious phenomena for the reflectance spectra with increasing incident angle are further investigated. One is the center of the reflectance band shifting toward shorter wavelengths, and the other one is the bandwidth of the reflectance band approaching narrower.[14)]

According to Snell's law, the propagation angles differ in the high (n_H) and low (n_L) refractive-index layers, the center of the reflectance band (λ_C) as a function of incident angle can be described as[15)]

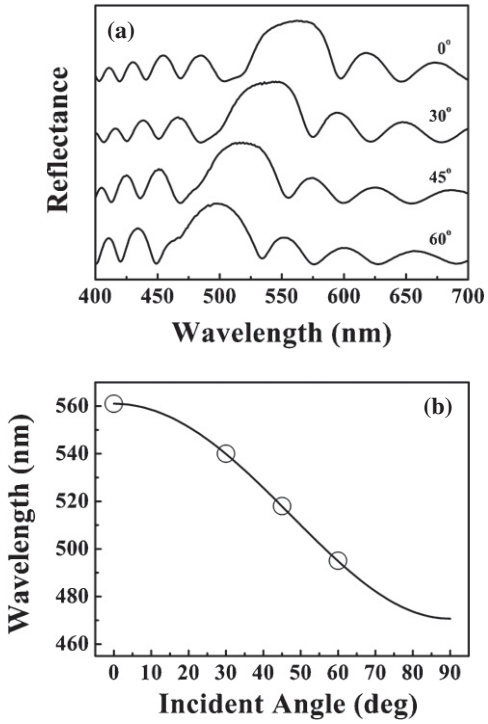

Fig. 2. (a) Incident angle-dependent reflectivity spectra of the ZnO/MgO multilayer films. (b) Theoretical solid curve calculated from Eq. (1) and the opened circles obtained from the experimental reflectance spectra.

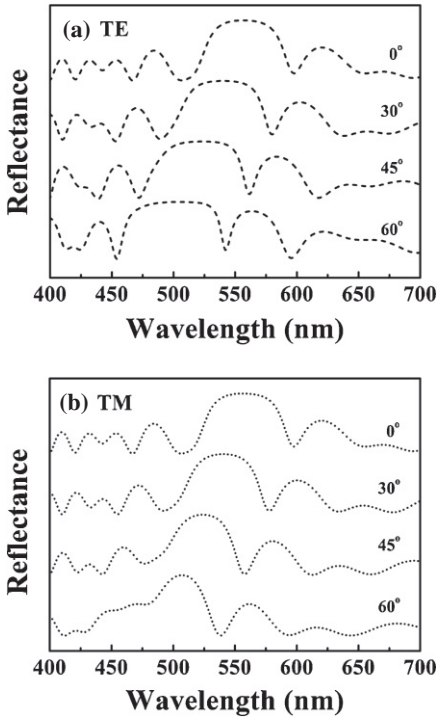

Fig. 3. Simulated reflectance spectra as a function of incident angle for (a) TE and (b) TM polarizations.

$$\lambda_C = \lambda_0[(1 - \sin^2\theta_i/{n_L}^2)^{1/2} + (1 - \sin^2\theta_i/{n_H}^2)^{1/2}], \quad (1)$$

where θ_i is the angle of incidence in the incident medium, which is assumed to be in the air, $n_i = 1$. The λ_0 is the center of the reflectance band at normal incidence. As shown in Fig. 2(b), the theoretical solid curve calculated from Eq. (1) and the opened circles obtained from the experimental reflectance spectra. It presents that the experimental data are in good agreement with the predicated center of the reflectance band as a function of incident angle.

The simulated reflectance spectra by using transfer matrix method are the following considered to understand the behavior of the resonance band depending on incident angle. At normal incidence, the fundamental transfer matrix without taking account of distinction between TE polarization and TM polarization is described as

$$\begin{pmatrix} M_{11} & M_{12} \\ M_{21} & M_{22} \end{pmatrix} = D_0^{-1}[D_H \cdot P_H \cdot D_H^{-1} \cdot D_L \cdot P_L \cdot D_L^{-1}]^N D_S, \quad (2)$$

where

$$P = \begin{bmatrix} e^{i\varphi} & 0 \\ 0 & -e^{i\varphi} \end{bmatrix} \quad \left(\varphi = \frac{2\pi nd}{\lambda}, d\text{: thickness}\right)$$

and

$$D = \begin{bmatrix} 1 & 1 \\ n & -n \end{bmatrix} \quad (n\text{: refractive index});$$

hence D_0, D_H, D_L, and D_S are the dynamic matrices for free space, ZnO, MgO, and Si substrate, respectively; P_H and P_L are the propagation matrices for ZnO and MgO, respectively; N is the number of periods.

To consider the theoretical reflectance spectrum at various incident angles for TE or TM polarized waves, the effective dynamic matrix used in the transfer matrix is

$$D_{TE} = \begin{bmatrix} 1 & 1 \\ n\cos\theta & -n\cos\theta \end{bmatrix}$$

for TE polarization and

$$D_{TM} = \begin{bmatrix} \cos\theta & -\cos\theta \\ n & -n \end{bmatrix}$$

for TM polarization.[16] The simulated results for TE and TM polarizations are plotted in Figs. 3(a) and 3(b), respectively. Both of the two curves exhibiting the increased angle of incidence shift the resonant frequency to shorter wavelength. However, the curves present that the TE bandwidth increases while the TM bandwidth decreases with increasing incident angle.[17] It also shows the significant enhancement and reduction in sharpness on the short-wavelength side of the reflectance band edge for TE and TM polarizations, respectively.

To discuss the variations in the reflection band as a function of incident angle, the wavelength edge (λ_E) of the reflection band can be given by[15]

$$\lambda_E = \lambda_C[1 \pm \Delta g], \quad (3)$$

$$\Delta g = \left(\frac{2}{\pi}\right)\sin^{-1}\left(\frac{\eta_H - \eta_L}{\eta_H + \eta_L}\right), \quad (4)$$

where Δg is modified from its usual normal-incidence definition to include the dependence on effective refractive-

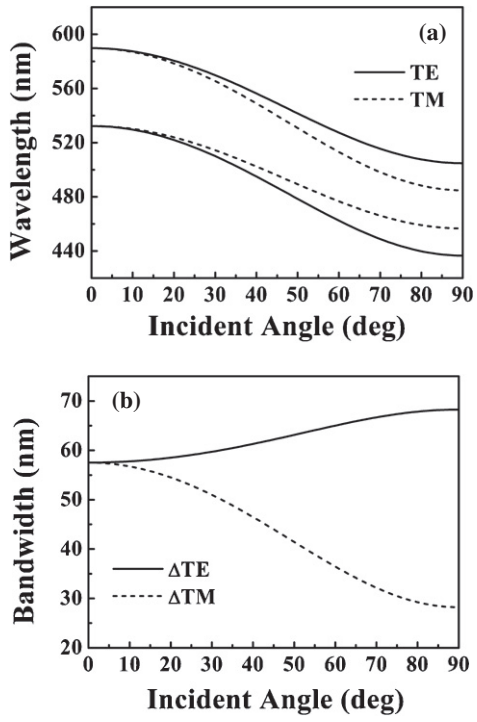

Fig. 4. (a) Long- and short-wavelength reflection band edges for TE (solid line) and TM (dashed line) polarizations. (b) Bandwidth as a function of incident angle for TE (solid line) and TM (dashed line) polarizations.

index values (η_H or η_L) to account for the different polarization states. The TE and TM effective refractive indices are presented as $\eta_{TE} = (n^2 - \sin^2\theta_i)^{1/2}$ and $\eta_{TM} = n^2/(n^2 - \sin^2\theta_i)^{1/2}$, respectively.[15] By calculating from Eqs. (3) and (4), the theoretical TE- and TM-reflection bands in terms of wavelength and incident angle are shown in Fig. 4(a). The variations in the bandwidth of the TE- and TM-reflection bands are also plotted in Fig. 4(b). The results present clearly the slowly broaden TE-reflection band and the dramatically narrowed TM-reflection band with increasing incident angle. The bandwidth value from the TM-reflection band at different incident angles is in good agreement with that estimated from the measured spectra, which suggests the actual reflectance band would be dominated mainly by TM polarization.

Additionally, a typical characterization of omnidirectional reflector, as mentioned above, cannot be observed in Fig. 2(a). It has been known that the long- and short-wavelength edges of omnidirectional-reflection band are defined by the longer-wavelength TM-reflection band at incident angle of 90° and the shorter-wavelength reflection band at 0°, respectively.[15,18] Therefore, as shown in Fig. 4(a), the calculated longer-wavelength TM-reflection band at incident angle of 90° being lower than the shorter-wavelength reflection band at 0° predicates no omnidirectional-reflection band in our designed ZnO/MgO multilayer structure.[18] Nevertheless, by theoretical simulation to design an omnidirectional-reflection band, we can find that the refractive index of material selected for being a high refractive index layer has to be larger than about 2.4, which is suggested to be a valuable parameter to fabricate a multilayer omnidirectional reflector.

4. Conclusion

In summary, we have investigated the incident-angle-dependent reflectance spectra of the 10-period ZnO/MgO multilayer films on Si fabricated by sputtering technique. The theoretical dispersion curves by using transfer matrix method taken account of TE and TM polarizations are calculated to clarify the measured reflectance spectra at different incident angles. There exists good agreement between the measured and simulated reflectance spectra as a function of incident angle. The simulated reflection band of TE and TM polarization can predicate the variations in the incident-angle-dependent resonance band, which indicates that the TM-reflection band would dominate significantly the performance of measured reflectance spectra.

Acknowledgement

The authors would like to acknowledge the support of the National Science Council Project No. NSC 102-2633-E-236-001 and 102-2221-E-272-006.

References

1) S. J. Pearton, D. P. Norton, K. Ip, Y. W. Heo, and T. Steiner: Superlattices Microstruct. **34** (2003) 3.
2) Ü. Özgür, Ya. I. Alivov, C. Liu, A. Teke, M. A. Reshchikov, S. Doğan, V. Avrutin, S.-J. Cho, and H. Morkoç: J. Appl. Phys. **98** (2005) 041301.
3) Y. J. Lu, C. X. Shan, M. M. Jiang, B. H. Li, K. W. Liu, R. G. Li, and D. Z. Shen: RSC Adv. **4** (2014) 16578.
4) S. Kalusniak, S. Sadofev, S. Halm, and F. Henneberger: Appl. Phys. Lett. **98** (2011) 011101.
5) C. B. Fu, C. S. Yang, M. C. Kuo, Y. J. Lai, J. Lee, J. L. Shen, W. C. Chou, and S. Jeng: Chin. J. Phys. **41** (2003) 535.
6) F. C. Peiris, S. Lee, U. Bindley, and J. K. Furdyna: Semicond. Sci. Technol. **14** (1999) 878.
7) Y. Fink, J. N. Winn, S. Fan, C. Chen, J. Michel, J. D. Joannopoulos, and E. L. Thomas: Science **282** (1998) 1679.
8) M. Kang, S. W. Kim, Y. G. Kim, and J. W. Ryu: J. Korean Phys. Soc. **57** (2010) 389.
9) C. W. Teng, J. F. Muth, Ü. Özgür, M. J. Bergmann, H. O. Everitt, A. K. Sharma, C. Jin, and J. Narayan: Appl. Phys. Lett. **76** (2000) 979.
10) N. B. Chen, H. Z. Wu, and T. N. Xu: J. Appl. Phys. **97** (2005) 023515.
11) Y. S. Huang, C. C. Chang, J. W. Lee, Y. C. Lee, C. C. Huang, Z. K. Wun, and K. K. Tiong: Phys. Scr. **T157** (2013) 014034.
12) T. S. Barros, B. S. Barros, Jr., S. Alves, R. H. A. G. Kiminami, H. L. Lira, and A. C. F. M. Costa: Mater. Sci. Forum **591–593** (2008) 745.
13) M. Sundrarajan, J. Suresh, and R. Rajiv Gandhi: Dig. J. Nanomater. Bios. **7** (2012) 983.
14) K. M. Chen, A. W. Sparks, H. C. Luan, D. R. Lim, K. Wada, and L. C. Kimerling: Appl. Phys. Lett. **75** (1999) 3805.
15) W. H. Southwell: Appl. Opt. **38** (1999) 5464.
16) P. Yeh: *Optical Waves in Layered Media* (Wiley, New York, 1988) p. 62.
17) Y. Park, Y. G. Roh, C. O. Cho, and H. Jeon: Appl. Phys. Lett. **82** (2003) 2770.
18) D. N. Chigrin, A. V. Lavrinenko, D. A. Yarotsky, and S. V. Gaponenko: Appl. Phys. A **68** (1999) 25.